

# Quantum generative adversarial network for generating discrete data

Haozhen Situ\*

*College of Mathematics and Informatics, South China Agricultural University, Guangzhou 510642, China*

Zhimin He†

*School of Electronic and Information Engineering, Foshan University, Foshan 528000, China*

Lvzhou Li‡

*School of Data and Computer Science, Sun Yat-Sen University, Guangzhou 510006, China*

Shenggen Zheng§

*Institute for Quantum Science and Engineering, Southern University of Science and Technology, Shenzhen 518055, China*

Generative adversarial network (GAN) is an effective machine learning framework to train unsupervised generative models, and has drawn lots of attention in recent years. In the GAN framework, the generator is trained by an adversarial discriminator, in order to generate new samples that follows the probability distribution of a given training dataset. Classical GANs cannot generate discrete data due to the requirement of differentiability on the design of generators. In this paper, we propose a quantum version of GAN for generation of discrete data, which complements classical GANs. Our quantum GAN is composed of a parameterized quantum circuit as the generator and a classical feedforward neural network as the discriminator. Two families of quantum circuits, both composed of simple one-qubit rotation and two-qubit controlled-phase gates, are considered. The analytic gradient of the quantum generator can be estimated by sampling the same quantum generator, so gradient-based methods can be used in the training. The results of a small-scale proof-of-principle numerical simulation demonstrates the effectiveness of our scheme.

## I. INTRODUCTION

The era of quantum computing is around the corner. In 2016, IBM provided access to its quantum computer to the community through a cloud platform called IBM Quantum Experience [1]. A quantum computing competition among IT giants including Microsoft, Google, Intel is under way. Because quantum computing has the admirable capability of processing exponentially high-dimensional data, quantum machine learning [2] is expected to be one of the most intriguing future applications of quantum computers. Many theoretical and experimental researches [3–13] on machines learning problems with the help of quantum computing have been taken in the last decade.

Designing explicit algorithms for artificial intelligence problems, *e.g.*, image and speech recognition, is very difficult or even impossible. Machine learning tries to solve these problems by parameterizing structured models and using empirical data to learn the parameters. There are two main classes of machine learning tasks, supervised learning and unsupervised learning. The goal of supervised learning is to build the relation between given data samples and their labels, while unsupervised learning aims at discovering the intrinsic patterns, properties or structures of unlabeled data samples. Compared with advanced supervised learning techniques, unsupervised learning is more intractable and challenging, because it requires one to efficiently represent, learn and sample from high-dimensional probability distributions [14].

Generative modelling is an important unsupervised learning subject, which aims to model the distribution of the training data and generate new data accordingly. Generative adversarial network (GAN) [15] is a new framework of training generative models and has drawn significant attention in recent years. The idea is to introduce a discriminator to play the role of the generator's adversary, so their competition forms a two-player game. The objective of the generator is to produce new samples resembling training samples, *a.k.a.*, real samples, while the objective of the discriminator is to distinguish real samples from generated ones, *a.k.a.*, fake samples. The process of training the discriminator and the generator alternately is described in Fig. 1. In step (a), the generator produces some fake

---

\*Electronic address: situhaozhen@gmail.com

†Electronic address: zhmihe@gmail.com

‡Electronic address: lilvzh@mail.sysu.edu.cn

§Electronic address: zhengsg@sustc.edu.cn

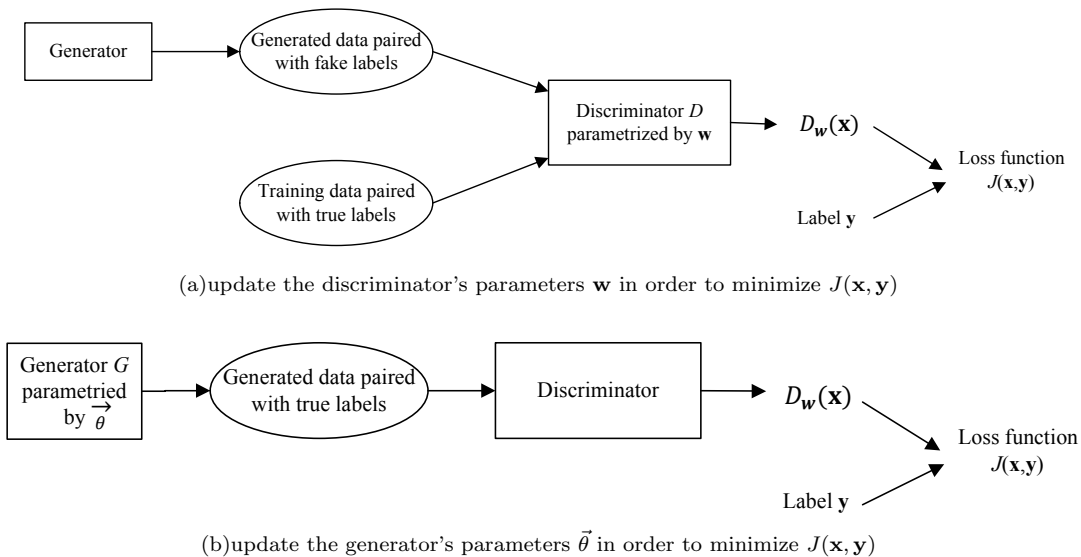


FIG. 1: Building blocks of generative adversarial network. Step (a) and (b) are alternately carried out until the generator outputs the same data distribution as the target distribution.

samples, then the discriminator is trained to distinguish between training data and generated data. The discriminator's parameters  $\mathbf{w}$  are updated in order to minimize a loss function  $J$ . The purpose of this step is to make the discriminator a better adversary, so the generator has to try harder to fool the discriminator. In step (b), the output samples of the generator are labeled as real and then fed into the discriminator. The generator's parameters  $\vec{\theta}$  are updated in order to minimize the loss function  $J$ , trying to make the discriminator believe the generated samples are real. After this step, the generator's ability improves a little bit. By repeating these two steps, the game will reach an equilibrium point, where the generator is able to generate the same statistics as the real samples and the prediction accuracy of the discriminator is  $1/2$ , not better than a random guess. Compared with other generative models with explicit likelihoods such as Boltzmann machines, belief networks and autoencoders, GAN as an implicit generative model can be more expressive due to less restrictions in network structures. Many variations of GAN have been proposed including conditional GAN [16], LAPGAN [17], DCGAN [18] and InfoGAN [19].

Recently the mergence of machine learning and quantum computing has developed into a hot topic, and some interesting results have been obtained [2]. Therefore, it is natural to consider how to improve the generative models with the help of quantum computing. Actually, some efforts have been devoted to this issue. For example, Ref. [20] trained shallow parameterized quantum circuits to generate GHZ states, coherent thermal states and Bars and Stripes images. Ref. [21] developed a gradient-based learning scheme to train deep parameterized quantum circuits for generation of Bars and Stripes images and mixture of Gaussian distributions. These quantum generative models are also known as Born machines as the output probabilities are determined by Born's rule [22]. In addition, the idea of quantum generative adversarial learning was recently explored theoretically in Ref. [23]. A quantum GAN consists of a quantum generator and a quantum discriminator was numerically implemented to generate simple quantum states [24]. Ref. [25] derived an adversarial algorithm for the problem of approximating an unknown quantum pure state. Ref. [26] demonstrated that a superconducting quantum circuit can be adversarially trained to replicate the statistics of the quantum data output from a digital qubit channel simulator.

Note that in the above works, parameterized quantum circuits were used as generative models. Also note that Ref. [27–31] used parameterized quantum circuits as machine learning parameterized models. Maybe one of the possible reasons for adopting parameterized quantum circuits is that sampling from output distributions of random quantum circuits must take exponential time in a classical computer [32], which suggests that quantum circuits exhibit stronger representational power than neural networks.

In this paper, we propose a quantum version of GAN composed of a parameterized quantum circuit as the quantum generator and a classical feedforward neural network as the classical discriminator. This quantum GAN can be trained by a hybrid quantum-classical gradient descent approach. Two families of parameterized quantum circuits are adopted as the generators. By a numerical simulation, we show that our scheme can effectively train these quantum circuits for generation tasks.

Compared with previous researches on quantum GANs [23–26] that focused on generating quantum data, our work

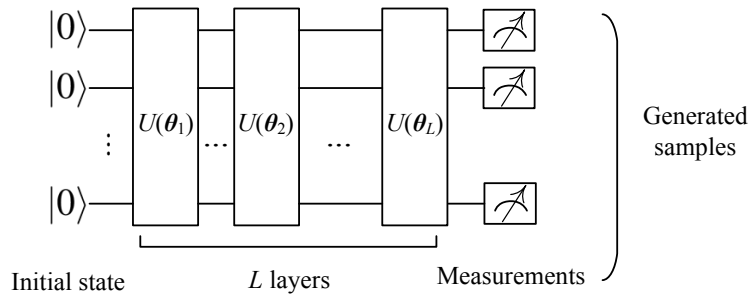


FIG. 2: The generative quantum circuit with  $L$  layers

centers on the generation of classical discrete data. We emphasize the fact that the outputs of quantum generators can be either quantum states, or classical discrete measurement outcomes. But there's no way to produce classical continuous data for a quantum circuit. On the other hand, classical GANs cannot produce discrete data such as one-hot word or character representations, because the only requirement on the design of generators by the GAN framework is that generators must be differentiable. Discrete data is non-differentiable so gradient descent update cannot directly be applied [33]. In contrast, we will show that the analytic gradient of the quantum generator can be estimated by sampling the same quantum generator with different parameters, settling the differentiable problem. As a complement to classical GANs, quantum GANs for generation of discrete data are worthy of research.

This paper is organized as follows. In section II, we present the constituents of the quantum generator and the classical discriminator. The loss function and optimization method are also described. Then the adversarial training algorithm is provided, together with the gradient estimation method for updating the parameters of the quantum generator. In section III, we report the numerical simulation that testify the effectiveness of our scheme. A brief conclusion follows in section IV.

## II. MODEL ARCHITECTURE AND TRAINING METHOD

In this section, we present the architecture of our generative quantum circuits built with simple one-qubit rotation and two-qubit controlled-phase gates, and the adversarial training scheme.

### A. Generative quantum circuit

Our quantum circuit for generation of  $N$ -bit samples involves  $N$  qubits, the layout of which is described in Fig. 2. The input quantum state is initialized to  $|0\rangle^{\otimes N}$ , and then passed through  $L$  layers of unitary operations. At the end of the circuit, all the qubits are measured in the computational basis. The measurement outcomes are gathered to form an  $N$ -bit sample  $x$ . Each layer is composed of several one-qubit rotation gates and two-qubit controlled-phase gates. Fig. 3 shows the arrangement of these gates in one layer. Three rotation operations are first applied to each qubit. This process can be written as

$$\prod_{i=1}^N R_z^i(\theta_{l,3}) R_x^i(\theta_{l,2}) R_z^i(\theta_{l,1}), \quad (1)$$

where the superscript  $i$  denotes the  $i$ th qubit, and the subscript  $l$  denotes the  $l$ th layer.  $R_x(\theta)$  and  $R_z(\theta)$  are rotation gates, *i.e.*,

$$R_x(\theta) = \begin{pmatrix} \cos \frac{\theta}{2} & -i \sin \frac{\theta}{2} \\ -i \sin \frac{\theta}{2} & \cos \frac{\theta}{2} \end{pmatrix}, R_z(\theta) = \begin{pmatrix} e^{-i\theta/2} & 0 \\ 0 & e^{i\theta/2} \end{pmatrix}. \quad (2)$$

The number of parameters/gates in this process is  $3N$  per layer. The choice of these operators is because any one-qubit unitary can be decomposed into this sequence of rotation operators [34].

We also need to entangle the qubits by performing controlled- $U$  gates between the qubits. This process can be

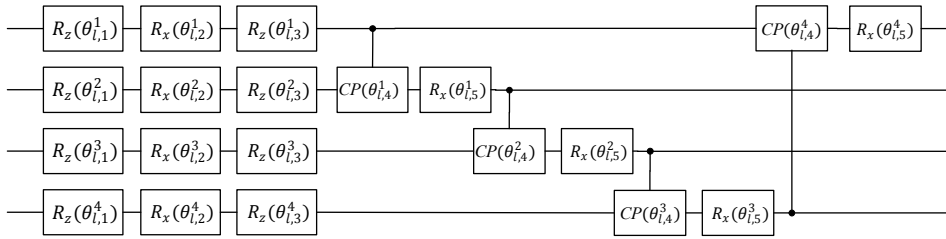


FIG. 3: A layer of the quantum circuit for four qubits

written as

$$\prod_{i=1}^N CU_{(i \bmod N)+1}^i, \quad (3)$$

where the superscript  $i$  denotes the control qubit, and the subscript  $(i \bmod N) + 1$  denotes the target qubit. Each unitary is characterized by three parameters, so the number of parameters in this process is  $3N$  per layer. However, Ref. [35] has pointed out that this process can be simplified to

$$\prod_{i=1}^N R_x^{(i \bmod N)+1}(\theta_{l,5}^i) CP_{(i \bmod N)+1}^i(\theta_{l,4}^i), \quad (4)$$

where

$$CP(\theta) = \begin{pmatrix} 1 & 0 & 0 & 0 \\ 0 & 1 & 0 & 0 \\ 0 & 0 & 1 & 0 \\ 0 & 0 & 0 & e^{i\theta} \end{pmatrix} \quad (5)$$

is the controlled-phase gate. Now the entangling process only has  $2N$  parameters/gates per layer. The total number of parameters/gates in the quantum circuit is  $5NL$ . The set of all parameters can be denoted as a vector  $\vec{\theta} = \{\theta_1, \dots, \theta_{5NL}\}$  for convenience of expression.

### B. Generative MPS quantum circuit

Besides the aforementioned family of quantum circuits, we also consider another family of quantum circuits, which are called ‘‘MPS quantum circuits’’ [36]. Fig. 4 illustrates the structure of the MPS quantum circuit, which looks like a maximally unbalanced tree with  $N$  nodes. Each node is a quantum ansatz which inputs and outputs  $V + 1$  qubits. The uppermost output qubit of each node is measured in the computational basis and the other  $V$  qubits flow to the next node. The  $N$  measurement outcomes comprise the  $N$ -bit generated sample  $x$ . Each node can contain  $L \geq 1$  layers which have the same gates and layouts as the layers depicted in Fig. 3. The number of parameters/gates in one node is  $5L(V + 1)$ , so the number of parameters/gates in an MPS quantum circuit is  $5NL(V + 1)$ . The input qubits are all initialized to  $|0\rangle$  in our numerical experiment.

If the MPS quantum circuit is implemented using quantum devices, each qubit that has been measured can be set to  $|0\rangle$  and reused as the input of the next node. So only  $V + 1$  qubits are actually needed in the circuit evaluation process. The sample dimension  $N$  is only related to the depth of the circuit. Fig. 5 gives an equivalent form of the MPS circuit in order to illustrate the idea of qubit recycling. This quantum circuit has advantage in physical implementation because near-term quantum devices have limited number of qubits.

### C. Discriminator

A discriminator  $D$  is introduced to distinguish between real samples and generated samples. The discriminator we use is a shallow feedforward neural network. The input layer has the same dimension as the samples. Only one hidden layer is employed. The output layer has only one output value in  $[0, 1]$ , which represents the discriminator’s prediction

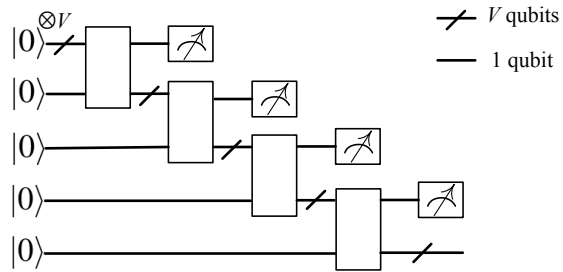
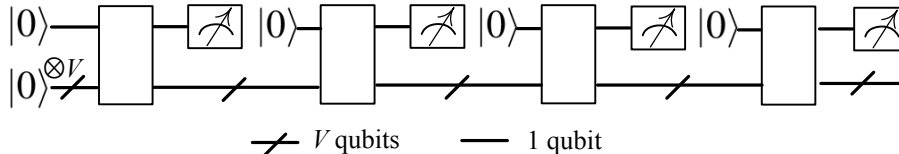
FIG. 4: The generative MPS quantum circuit with  $N = 4$  nodes

FIG. 5: The generative MPS quantum circuit with reused qubits

about the probability of the input sample being real. An output  $D(x) = 1$  means the discriminator believes the input sample  $x$  is definitely real, while an output  $D(x) = 0$  means it believes the input sample  $x$  is definitely fake.

The loss function of the discriminator we adopt here is the binary cross entropy function commonly used in binary classification tasks:

$$J_D = -\frac{1}{2} \left( \mathbb{E}_{x \sim P_d(x)} \log D(x) + \mathbb{E}_{x \sim P_{\tilde{g}}(x)} \log (1 - D(x)) \right), \quad (6)$$

where  $P_d(x)$  is the real data distribution and  $P_{\tilde{g}}(x)$  is the generated distribution. In every epoch of the training process, we sample one mini-batch of samples from the training data and the generator, respectively, to calculate the average loss

$$J_D(\mathbf{x}, \mathbf{y}) = -\frac{1}{2 \cdot \mathbf{batch\_D}} \sum_i y_i \log D(x_i) + (1 - y_i) \log(1 - D(x_i)), \quad (7)$$

where  $\mathbf{batch\_D}$  denotes the number of samples in one mini-batch,  $(x_i, y_i) \in (\mathbf{x}, \mathbf{y})$  denotes the  $i$ th sample and its label,  $y_i = 1(0)$  for real (fake) labels. The loss function evaluates how close are the predictions  $D(x_i)$  and the desired labels  $y_i$ .  $J_D(\mathbf{x}, \mathbf{y})$  achieves minimum zero if  $D(x_i) = y_i$  for every  $(x_i, y_i)$ .

Let  $\mathbf{w}$  be the set of all the parameters of the discriminator. The gradient of  $J_D(\mathbf{x}, \mathbf{y})$  with respect to  $\mathbf{w}$  can be obtained by the backpropagation algorithm. A variety of gradient-based optimization algorithms can be used to train the discriminator. For example, the vanilla gradient descent method updates  $\mathbf{w}$  in the following way:

$$\mathbf{w} \leftarrow \mathbf{w} - \alpha_D \cdot \frac{\partial J_D(\mathbf{x}, \mathbf{y})}{\partial \mathbf{w}}, \quad (8)$$

where  $\alpha_D$  is the learning rate.

#### D. Optimization of the generator parameters

The goal of the generator is to generate samples that can fool the discriminator. The training process of the generator only uses generated samples, which are paired with true labels, so Eq. (6) reduces to

$$J_G = -\mathbb{E}_{x \sim P_{\tilde{g}}(x)} \log D(x), \quad (9)$$

where  $P_{\tilde{g}}(x)$  is the probability of getting measurement outcome  $x$  from the quantum circuit parameterized with  $\vec{\theta} = \{\theta_1, \theta_2, \dots\}$ . The gradient of  $J_G$  with respect to  $\theta_i$  is

$$\frac{\partial J_G}{\partial \theta_i} = - \sum_{x \in \{0,1\}^N} \log D(x) \frac{\partial P_{\tilde{g}}(x)}{\partial \theta_i}. \quad (10)$$

---

**Algorithm 1** Adversarial training algorithm of our quantum GAN

---

**Input:**  $L$ : number of layers;  $V$ : number of ancilla qubits (only for MPS circuits); **batch\_D**, **batch\_G**: mini-batch size; **d\_step**: times of updating  $\mathbf{w}$  in one epoch; **g\_step**: times of updating  $\vec{\theta}$  in one epoch;

**Output:**  $\vec{\theta}$ : the parameters of the generator

- 1: Initialize the generator and the discriminator with random parameters
- 2: **for** number of training epoches **do**
- 3:   **for** **d\_step** steps **do**
- 4:     Sample a mini-batch of **batch\_D** samples from the training dataset. Label them as “real”.
- 5:     Sample a mini-batch of **batch\_D** samples from the quantum circuit. Label them as “fake”.
- 6:     Use these samples and labels to calculate the gradient of the loss according to Eq. (7).
- 7:     Update the discriminator’s parameters  $\mathbf{w}$  according to the gradient.
- 8:   **end for**
- 9:   **for** **g\_step** steps **do**
- 10:     For each  $\theta_i$ , sample a mini-batch of **batch\_G** samples from the quantum circuit with parameters  $\vec{\theta}^+$ .
- 11:     For each  $\theta_i$ , sample a mini-batch of **batch\_G** samples from the quantum circuit with parameters  $\vec{\theta}^-$ .
- 12:     Use these samples to calculate the gradient of the loss according to Eq. (13).
- 13:     Update the generator’s parameters  $\vec{\theta}$  according to the gradient.
- 14:   **end for**
- 15: **end for**

---

Using the techniques in Ref. [29] we have

$$\frac{\partial P_{\vec{\theta}}(x)}{\partial \theta_i} = \frac{1}{2} (P_{\vec{\theta}^+}(x) - P_{\vec{\theta}^-}(x)), \quad (11)$$

where  $\vec{\theta}^{\pm} = \vec{\theta} \pm \frac{\pi}{2} \mathbf{e}^i$ ,  $\mathbf{e}^i$  is the  $i$ th unit vector in the parameter space (i.e.,  $\theta_i \leftarrow \theta_i \pm \frac{\pi}{2}$ , with other angles unchanged). The proof is given in the appendix. By substituting Eq. (11) into Eq. (10), we have

$$\frac{\partial J_G}{\partial \theta_i} = \frac{1}{2} \mathbb{E}_{x \sim P_{\vec{\theta}^-}(x)} \log D(x) - \frac{1}{2} \mathbb{E}_{x \sim P_{\vec{\theta}^+}(x)} \log D(x). \quad (12)$$

In order to estimate the gradient with respect to each  $\theta_i$ , we have to sample two mini-batches  $\mathbf{x}_i^+$  and  $\mathbf{x}_i^-$  from the circuits with parameters  $\vec{\theta}^+$  and  $\vec{\theta}^-$ , respectively, then the gradient is estimated by

$$\frac{1}{2 \cdot \text{batch\_G}} \left( \sum_{x \in \mathbf{x}_i^-} \log D(x) - \sum_{x \in \mathbf{x}_i^+} \log D(x) \right), \quad (13)$$

where **batch\_G** denotes the number of samples in one mini-batch.

The generator’s parameters  $\vec{\theta}$  can be optimized by gradient-based optimization algorithms. For example, the vanilla gradient descent method updates  $\vec{\theta}$  in the following way:

$$\vec{\theta} \leftarrow \vec{\theta} - \alpha_G \cdot \frac{\partial J_G}{\partial \vec{\theta}}, \quad (14)$$

where  $\alpha_G$  is the learning rate.

### E. Adversarial training

The adversarial training algorithm of our quantum GAN is described in Algorithm 1. The training process iterates for a fixed number of epoches, or until some stopping criterion is reached, *e.g.*, convergence on the loss function. At each epoch, the parameters of the discriminator and the generator are updated **d\_step** and **g\_step** times, respectively.

## III. NUMERICAL SIMULATION

We verify our proposal using a synthetic dataset known as Bars and Stripes (BAS), which is also used in Ref. [20, 21] to test quantum generative models. The dataset contains  $m \times m$  binary images with only bar patterns or

stripe patterns. There are  $2^m$  different vertical bar patterns and  $2^m$  different horizontal stripe patterns. The all-black and all-white patterns are counted in both bar patterns and stripe patterns. So there are  $2^{m+1} - 2$  possible BAS patterns for an  $m \times m$  image. We assume all BAS patterns appear with equal probability. Obviously each pixel can be encoded in one qubit, so an  $m \times m$  image can be encoded in  $m^2$  qubits. We restrict our experiments to the case of  $m = 2$ , because it's difficult to simulate more qubits efficiently using an ordinary PC. Experiments for larger  $m$  will be done in the future if an intermediate-scale near-term quantum device is available.

The simulation code is written in Python language. The discriminator is classical so it's implemented using the widely used deep learning framework PyTorch [37]. The discriminator has one input layer with dimension  $m \times m$ , one hidden layer made up of 50 neurons with the ReLU activation function  $f(x) = \max(0, x)$ , and one output neuron using the Sigmoid activation function  $f(x) = 1/(1+e^{-x})$ . The stochastic gradient optimizer Adam (Adaptive Moment Estimation) [38] is used to update the discriminator's parameters. The initial learning rate for Adam is  $10^{-3}$ .

The generative quantum circuit is simulated directly by calculating the evolution of the wavefunction. An  $N$ -qubit wavefunction is encoded in a  $2^N$ -dimensional complex vector. After performing a single-qubit operation  $u_{11}|0\rangle\langle 0| + u_{12}|0\rangle\langle 1| + u_{21}|1\rangle\langle 0| + u_{22}|1\rangle\langle 1|$  on the  $i$ th qubit, the wavefunction is transformed to

$$\begin{aligned}\alpha'_{*...*0_i*...*} &= u_{11} \cdot \alpha_{*...*0_i*...*} + u_{12} \cdot \alpha_{*...*1_i*...*}, \\ \alpha'_{*...*1_i*...*} &= u_{21} \cdot \alpha_{*...*0_i*...*} + u_{22} \cdot \alpha_{*...*1_i*...*},\end{aligned}\tag{15}$$

where  $\alpha$  and  $\alpha'$  are amplitudes before and after transformation. The case of two-qubit operation can be deduced analogously. The parameters of the quantum circuit is updated according to Eq. (14) with a constant learning rate  $\alpha_G = 2 \times 10^{-2}$ . The gradient is estimated according to Eq. (13).

The two numerical experiments we perform differ in the structure of the quantum generator. The first experiment uses the general quantum circuit described in section II A, while the second experiment uses the MPS quantum circuit described in section II B.

### A. Numerical experiment 1

In the first numerical experiment, the quantum generator is the general quantum circuit presented in section II A. After a lot of trials, we choose the hyper-parameters **batch\_D** = 64, **batch\_G** = 100, **d\_step** = 1, **g\_step** = 1. The learnable parameters of the quantum circuit are randomly initialized in the interval  $(-\pi, \pi)$ . Unlike the training of classification models, the stopping criterion of training GANs is very tricky, so we simply run the training algorithm for 5000 epoches. For each  $L = 1, 2, 3, 4, 5, 6$ , we repeat the experiment 30 times. The averages and standard deviations of three indicators (i.e., accuracy, KL divergence and loss) are reported every 50 epoches.

We first examine the accuracy of the generator. The accuracy in some epoch is defined as the ratio of the number of valid samples (i.e., BAS patterns) in one mini-batch to **batch\_D**. The generator accuracy w.r.t. the number of epoches is depicted in Fig. 6. We can see that for each  $L$  from 1 to 6, the accuracy increases very quickly and achieves nearly 100% in 1000 epoches, which means that it's not difficult for the generator to learn to avoid producing non-BAS patterns.

But our goal is not merely producing correct BAS patterns. The distribution of the generated patterns is expected to be the same as that of the training dataset, i.e., uniform distribution in our case. KL divergence is usually used to measure how one probability distribution diverges from a second, expected probability distribution, which is defined by

$$\text{KLD}(P_d \| P_{\hat{\theta}}) = - \sum_x P_d(x) \log \frac{P_{\hat{\theta}}(x)}{P_d(x)},\tag{16}$$

where  $P_d$  and  $P_{\hat{\theta}}$  are the real data distribution and the generated distribution, respectively.  $\text{KLD}(P_d \| P_{\hat{\theta}})$  is non-negative and equals zero if and only if  $P_d = P_{\hat{\theta}}$  almost everywhere. The distribution of the generated samples can be estimated by their frequency of occurrences. In numerical simulation, the exact distribution can be obtained from the wave function. We draw the variation of the KL divergence w.r.t. the number of epoches in Fig. 7. For  $L = 1, 2$ , the capacity of the generator is not enough for generating the target distribution. A large standard deviation means in some runs the generator can produce the target distribution, but in other runs it can generate only part of the valid BAS patterns. For  $L = 3$ , the trained generator can generate the target distribution in most of the 30 runs. For  $L = 4, 5, 6$ , the KL divergence always converges to zero, which demonstrates the representation power of deeper quantum circuits.

We also plot the loss functions of both the generator and the discriminator w.r.t. the number of epoches in Fig. 8. When the adversarial game reaches equilibrium, the output of the discriminator is 1/2 for both real and generated

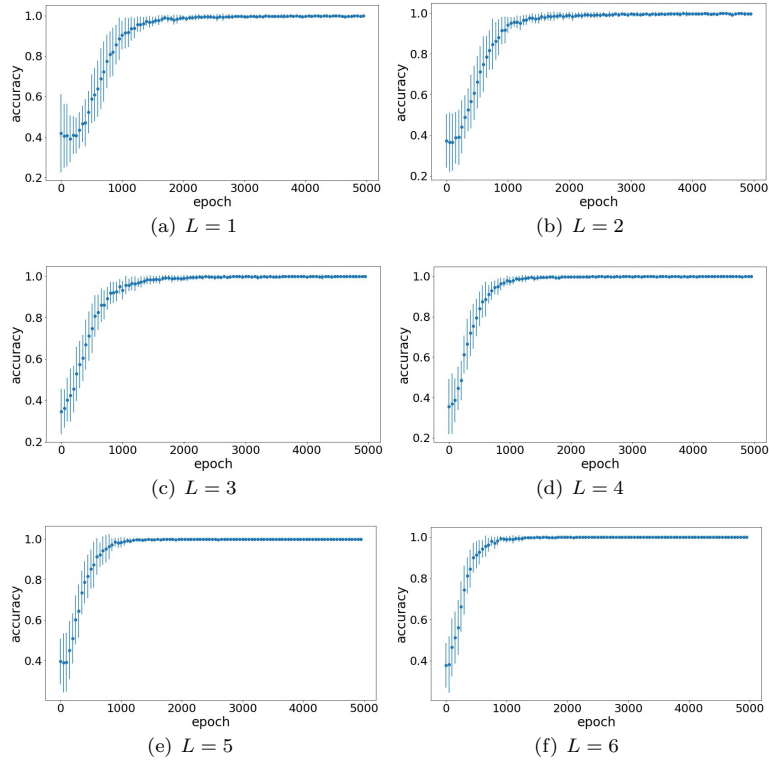


FIG. 6: Averages and standard deviations of the accuracy w.r.t. the number of epoches

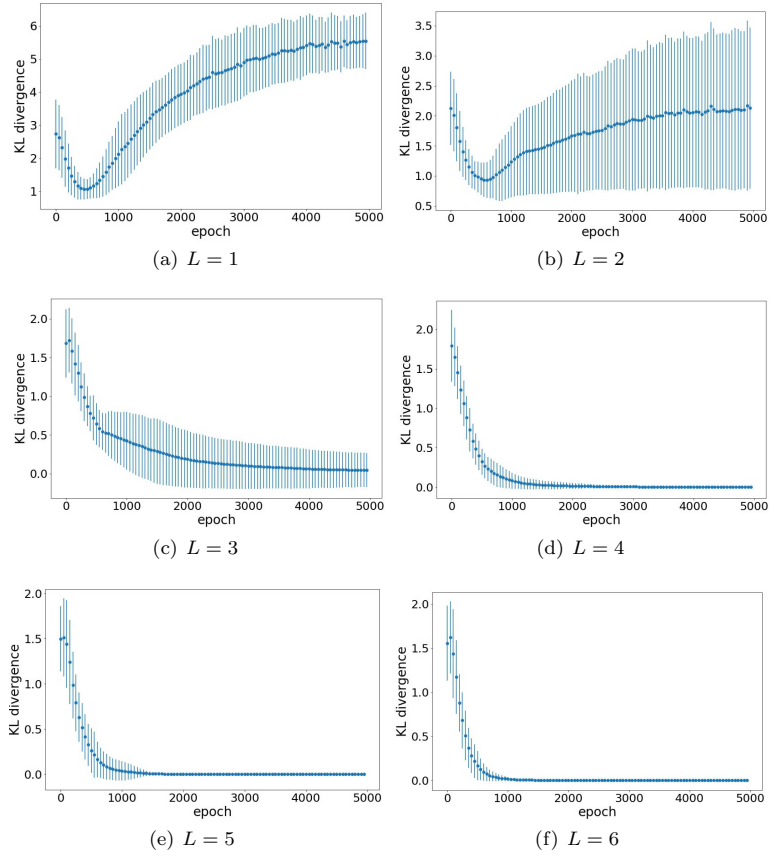


FIG. 7: Averages and standard deviations of the KL divergence w.r.t. the number of epoches



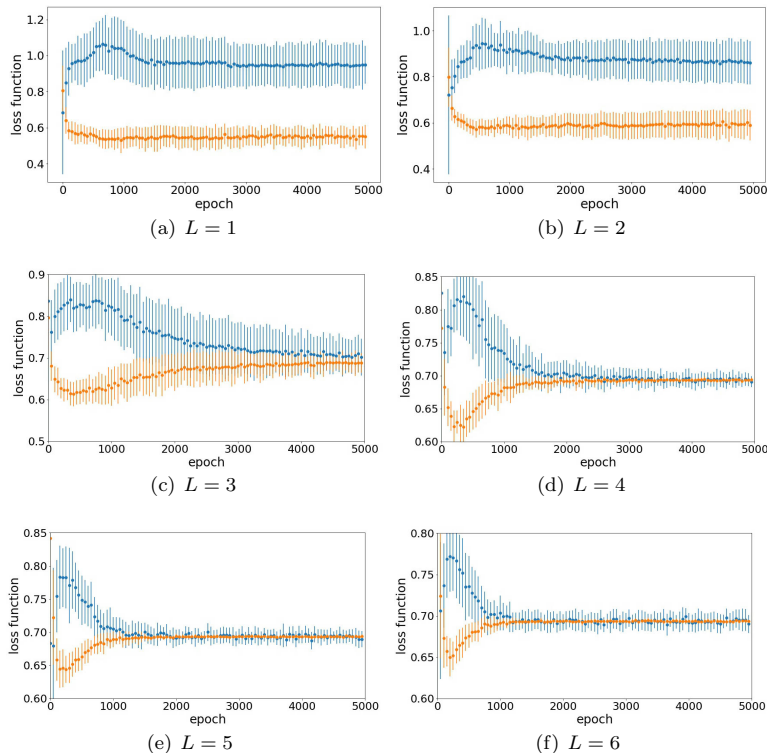


FIG. 8: Averages and standard deviations of the loss functions of the generator (in blue) and the discriminator (in orange) w.r.t. the number of epochs

samples. By substituting  $D(x_i) = 1/2$  into Eq. (7), we have  $J_{final} = -\log \frac{1}{2} \approx 0.693$ . From Fig. 8 we can see that for  $L = 1, 2$ , the averages of two loss functions are separated. With the increase of  $L$ , they gradually converge to  $J_{final}$ .

## B. Numerical experiment 2

In the second numerical experiment, the quantum generator is the MPS quantum circuit presented in section II B. After a lot of trials, we choose the hyper-parameters **batch\_D** = 64, **batch\_G** = 100, **d\_step** = 1, **g\_step** = 1. The learnable parameters of the quantum circuit are randomly initialized in the interval  $(-\pi, \pi)$ . We report 4 cases with  $L$  and  $V$  set to: (a)  $L = 2, V = 1$ , (b)  $L = 2, V = 2$ , (c)  $L = 2, V = 3$ , (d)  $L = 3, V = 2$ . Because the amount of learnable parameters in the MPS circuit is  $5NL(V + 1)$ , the number of parameters in these four cases is 80, 120, 160 and 180, respectively. A model with more parameters can be regarded as having larger capacity. For each case, we repeat the experiment 30 times and report the averages and standard deviations every 50 epochs.

The generator accuracy w.r.t. the number of epoches is depicted in Fig. 9, which shows that the accuracy increases very quickly and achieves nearly 100% after 1000 epoches. The variation of the KL divergence is depicted in Fig. 10. We can see that the generated distribution gradually approaches the real data distribution with the increase of the capacity of the generator. The variation of the loss functions of both the generator and the discriminator w.r.t. the number of epoches is plotted in Fig. 11. We can see that both loss functions converge to  $J_{final}$  when the KL divergence approaches zero.

## IV. CONCLUSION

Researches on quantum versions of GANs seem very promising, due to the great potential and applications of GANs in machine learning and the advantage of quantum computing. In this paper, we propose a quantum GAN for generation of classical discrete data. By numerical simulation, we show our quantum GAN can generate simple BAS data distribution effectively. The requirement of differentiability on the design of generators by the GAN framework implies that classical GANs cannot produce discrete data. However, there's a delicate way to estimate the analytic

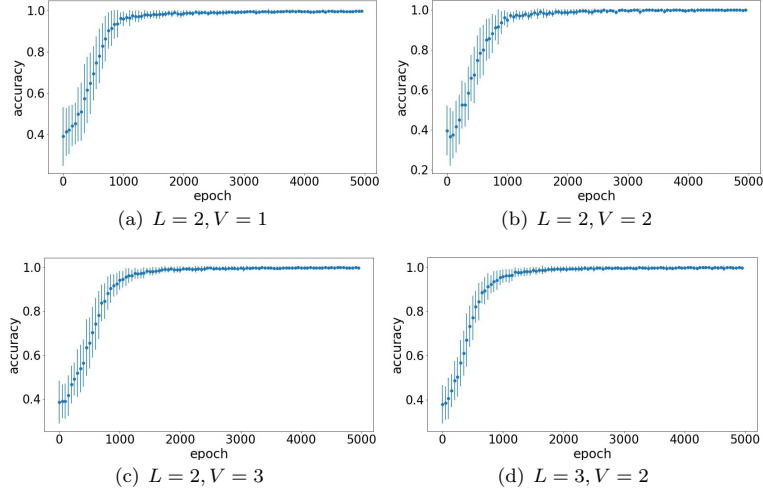


FIG. 9: Averages and standard deviations of the accuracy w.r.t. the number of epochs

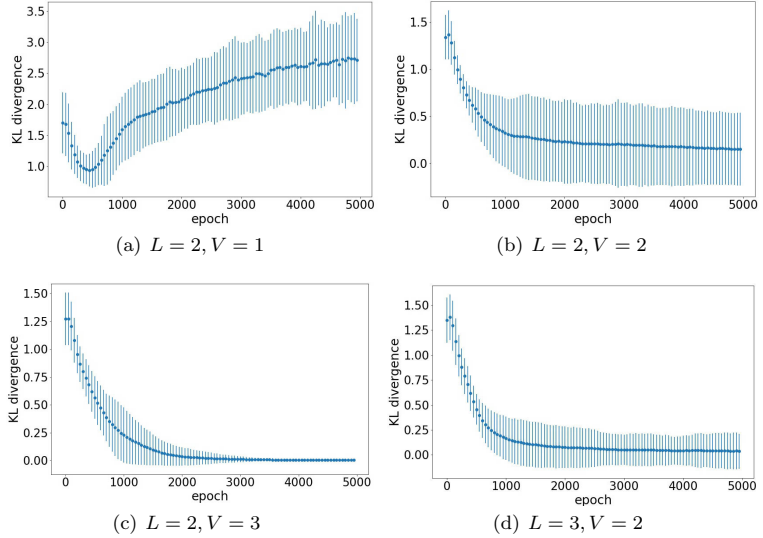


FIG. 10: Averages and standard deviations of the KL divergence w.r.t. the number of epochs

gradient of the quantum generator by sampling the same quantum generator with different parameters. So quantum GANs for generation of discrete data can be regarded as a complement to classical GANs and deserve further research.

Interesting future research directions include generating discrete data with higher dimension, choosing the layout of the generative quantum circuit, modelling the generator with non-unitary quantum dynamics, employing variants of GAN framework, using more heuristics to guide the training, and in-depth theoretical analysis of quantum GANs.

*Note* - After our work was completed, we found that some researchers were also interested in this topic and wrote a similar manuscript [39].

### Acknowledgement

This work is supported by the National Natural Science Foundation of China (Nos. 61772565, 61802061, 61502179, 61602532, 61472452), the Fundamental Research Funds for the Central Universities (No. 17lgzd29), the Natural Science Foundation of Guangdong Province of China (No. 2017A030313378), the Project of Department of Education of Guangdong Province (No.2017KQNCX216), the Science and Technology Program of Guangzhou City of China (No. 201707010194), and the Research Foundation for Talented Scholars of Foshan University (No. gg040996).

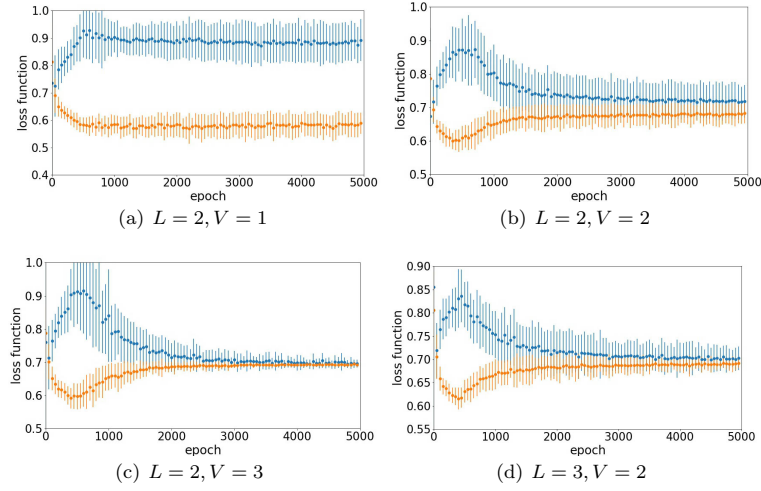


FIG. 11: Averages and standard deviations of the loss functions of the generator (in blue) and the discriminator (in orange) w.r.t. the number of epoches

### Appendix

This appendix gives the proof of Eq. (11), which makes use of the following formulas:

$$\frac{\partial ABC}{\partial \theta} = A \frac{\partial B}{\partial \theta} C, \quad (\text{A.1})$$

$$\frac{\partial A \otimes B \otimes C}{\partial \theta} = A \otimes \frac{\partial B}{\partial \theta} \otimes C, \quad (\text{A.2})$$

where the parameter  $\theta$  appears in operator  $B$  but not in  $A$  or  $C$ . Another useful formula is

$$\frac{\partial AB}{\partial \theta} = \frac{\partial A}{\partial \theta} B + A \frac{\partial B}{\partial \theta}, \quad (\text{A.3})$$

where the parameter  $\theta$  appears in both operators  $A$  and  $B$ . The above formulas can be proved directly by using the definitions of matrix multiplication and tensor product.

Suppose the quantum circuit has  $k$  gates which can be denoted as  $U_j$  with  $j \in \{1, \dots, k\}$ . For an initial state  $\rho_0$ , the output of the quantum circuit is  $U_{k:1} \rho_0 U_{k:1}^\dagger$ , where the notation  $U_{k:1} = U_k \dots U_1$  is introduced for convenience. Suppose  $\theta$  is a parameter that appears and only appears in  $U_j$ , the partial derivative of  $P_{\bar{\theta}}(x)$  with respect to  $\theta$  is

$$\begin{aligned} \frac{\partial P_{\bar{\theta}}(x)}{\partial \theta} &= \frac{\partial}{\partial \theta} \langle x | U_{k:1} \rho_0 U_{k:1}^\dagger | x \rangle \\ &= \langle x | U_{k:j+1} \frac{\partial U_j}{\partial \theta} U_{j-1:1} \rho_0 U_{k:1}^\dagger | x \rangle + \langle x | U_{k:1} \rho_0 U_{j-1:1}^\dagger \frac{\partial U_j^\dagger}{\partial \theta} U_{k:j+1}^\dagger | x \rangle. \end{aligned} \quad (\text{A.4})$$

For  $U_j$  and  $U_j^\dagger$  being a controlled-phase gate and its Hermitian conjugate, the gradients are  $\frac{\partial U_j}{\partial \theta} = i|11\rangle\langle 11|U_j$  and  $\frac{\partial U_j^\dagger}{\partial \theta} = -iU_j^\dagger|11\rangle\langle 11|$ , respectively. By substituting them into Eq. (A.4), we have

$$\begin{aligned} \frac{\partial P_{\bar{\theta}}(x)}{\partial \theta} &= i \langle x | U_{k:j+1} | 11 \rangle \langle 11 | U_{j:1} \rho_0 U_{k:1}^\dagger | x \rangle - i \langle x | U_{k:1} \rho_0 U_{j:1}^\dagger | 11 \rangle \langle 11 | U_{k:j+1}^\dagger | x \rangle \\ &= i \langle x | U_{k:j+1} [ | 11 \rangle \langle 11 |, U_{j:1} \rho_0 U_{j:1}^\dagger ] U_{k:j+1}^\dagger | x \rangle. \end{aligned} \quad (\text{A.5})$$

The following property of the commutator for an arbitrary operator  $\rho$

$$[ | 11 \rangle \langle 11 |, \rho ] = -\frac{i}{2} \left( U_j \left( \frac{\pi}{2} \right) \rho U_j^\dagger \left( \frac{\pi}{2} \right) - U_j \left( -\frac{\pi}{2} \right) \rho U_j^\dagger \left( -\frac{\pi}{2} \right) \right) \quad (\text{A.6})$$

can be verified by the substitution of  $U_j(\frac{\pi}{2}) = I + (i - 1)|11\rangle\langle 11|$  and  $U_j(-\frac{\pi}{2}) = I - (1 + i)|11\rangle\langle 11|$ . By substituting Eq. (A.6) into Eq. (A.5), we have

$$\begin{aligned} \frac{\partial P_{\bar{\theta}}(x)}{\partial \theta} &= \frac{1}{2} \left( \langle x | U_{k:j+1} U_j(\theta + \frac{\pi}{2}) U_{j-1:1} \rho_0 U_{j-1:1}^\dagger U_j^\dagger(\theta + \frac{\pi}{2}) U_{k:j+1}^\dagger | x \rangle \right. \\ &\quad \left. - \langle x | U_{k:j+1} U_j(\theta - \frac{\pi}{2}) U_{j-1:1} \rho_0 U_{j-1:1}^\dagger U_j^\dagger(\theta - \frac{\pi}{2}) U_{k:j+1}^\dagger | x \rangle \right) \\ &= \frac{1}{2} (P_{\bar{\theta}^+}(x) - P_{\bar{\theta}^-}(x)). \end{aligned} \tag{A.7}$$

So the proof for the case of controlled-phase gates is finished. For  $U_j$  being the rotation gates  $R_x$ ,  $R_y$  or  $R_z$ , the proof has been given in [29]. Our circuit architecture only contains controlled-phase gates and rotation gates, so the whole proof is finished.

- 
- [1] IBM Quantum Experience: <http://www.research.ibm.com/ibm-q/>
- [2] J. Biamonte, P. Wittek, N. Pancotti, P. Rebentrost, N. Wiebe, and S. Lloyd, Quantum machine learning, *Nature* 549, 195 (2017).
- [3] A.W. Harrow, A. Hassidim, and S. Lloyd, Quantum algorithm for linear systems of equations, *Phys. Rev. Lett.* 103, 150502 (2009).
- [4] N. Wiebe, D. Braun, and S. Lloyd, Quantum algorithm for data fitting, *Phys. Rev. Lett.* 109, 050505 (2012).
- [5] X.D. Cai, C. Weedbrook, Z.E. Su, M.C. Chen, M. Gu, M.J. Zhu, L. Li, N.L. Liu, C.Y. Lu, and J.W. Pan, Experimental quantum computing to solve systems of linear equations, *Phys. Rev. Lett.* 110, 230501 (2013).
- [6] P. Rebentrost, M. Mohseni, and S. Lloyd, Quantum support vector machine for big data classification, *Phys. Rev. Lett.* 113, 130503 (2014).
- [7] S. Lloyd, M. Mohseni, and P. Rebentrost, Quantum principal component analysis, *Nat. Phys.* 10, 631 (2014).
- [8] X.D. Cai, D. Wu, Z.E. Su, M.C. Chen, X.L. Wang, L. Li, N.L. Liu, C.Y. Lu, and J.W. Pan, Entanglement-based machine learning on a quantum computer, *Phys. Rev. Lett.* 114, 110504 (2015).
- [9] C.H. Yu, F. Gao, Q.L. Wang, and Q.Y. Wen, Quantum algorithm for association rules mining, *Phys. Rev. A* 94, 042311 (2016).
- [10] V. Dunjko, J.M. Taylor, and H.J. Briegel, Quantum-enhanced machine learning, *Phys. Rev. Lett.* 117, 130501 (2016).
- [11] A. Monràs, G. Sentís, and P. Wittek, Inductive supervised quantum learning, *Phys. Rev. Lett.* 118, 190503 (2017).
- [12] B.J. Duan, J.B. Yuan, Y. Liu, and D. Li, Quantum algorithm for support matrix machines, *Phys. Rev. A* 96, 032301 (2017).
- [13] C.H. Yu, F. Gao, C.H. Liu, D. Huynh, M. Reynolds, and J.B. Wang, Quantum algorithm for visual tracking, arXiv: 1807.00476.
- [14] I. Goodfellow, Y. Bengio, and A. Courville, *Deep Learning*, MIT Press (2016)
- [15] I. Goodfellow, J. Pouget-Abadie, M. Mirza, B. Xu, D. Warde-Farley, S. Ozair, A. Courville, and Y. Bengio, Generative adversarial nets, in *Proceedings of the 27th International Conference on Neural Information Processing Systems* (2014) pp. 2672-2680.
- [16] M. Mirza and S. Osindero, Conditional generative adversarial nets, arXiv: 1411.1784.
- [17] E. Denton, S. Chintala, A. Szlam, and R. Fergus, Deep generative image models using a Laplacian pyramid of adversarial networks, in *Proceedings of the 29th International Conference on Neural Information Processing Systems* (2015) pp. 1486-1494.
- [18] A. Radford, L. Metz, and S. Chintala, Unsupervised representation learning with deep convolutional generative adversarial networks, arXiv: 1511.06434.
- [19] X. Chen, Y. Duan, R. Houthoofd, J. Schulman, I. Sutskever, and P. Abbeel, Infogan: Interpretable representation learning by information maximizing generative adversarial nets, in *Proceedings of the 30th International Conference on Neural Information Processing Systems* (2016) pp. 2172-2180.
- [20] M. Benedetti, D. Garcia-Pintos, Y. Nam, and A. Perdomo-Ortiz, A generative modeling approach for benchmarking and training shallow quantum circuits, arXiv: 1801.07686.
- [21] J.G. Liu and L. Wang, Differentiable learning of quantum circuit Born machine, arXiv: 1804.04168.
- [22] M. Born, *Zur Quantenmechanik der Stoßvorgänge*, *Z. Phys.* 37, 863 (1926).
- [23] S. Lloyd and C. Weedbrook, Quantum generative adversarial learning, *Phys. Rev. Lett.* 121, 040502 (2018).
- [24] P. Dallaire-Demers and N. Killoran, Quantum generative adversarial networks, *Phys. Rev. A* 98, 012324 (2018).
- [25] M. Benedetti, E. Grant, L. Wossnig, and S. Severini, Adversarial quantum circuit learning for pure state approximation, arXiv: 1806.00463.
- [26] L. Hu, S.H. Wu, W.Z. Cai et al., Quantum generative adversarial learning in a superconducting quantum circuit, arXiv: 1808.02893.
- [27] K.H. Wan, O. Dahlsten, H. Kristjánsson, R. Gardner, and M.S. Kim, Quantum generalisation of feedforward neural networks, *npj Quantum Information* 3, 36 (2017).

- [28] J. Romero, J.P. Olson, and A. Aspuru-Guzik, Quantum autoencoders for efficient compression of quantum data, *Quantum Sci. and Technol.* 2, 045001 (2017).
- [29] K. Mitarai, M. Negoro, M. Kitagawa, and K. Fujii, Quantum circuit learning, *Phys. Rev. A* 98, 032309 (2018).
- [30] L. Cincio, Y. Subasi, A.T. Sornborger, and R.J. Coles, Learning the quantum algorithm for state overlap, *New J. Phys.* 20, 113022 (2018).
- [31] L. Lamata, U. Alvarez-Rodriguez, J.D. Martín-Guerrero, M. Sanz, and E. Solano, Quantum autoencoders via quantum adders with genetic algorithms, *Quantum Sci. and Technol.* 4, 014007 (2019).
- [32] S. Boixo, S.V. Isakov, V.N. Smelyanskiy, R. Babbush, N. Ding, Z. Jiang, M.J. Bremner, J.M. Martinis, and H. Neven, Characterizing quantum supremacy in near-term devices, *Nat. Phys.* 14, 595 (2018).
- [33] I. Goodfellow, NIPS 2016 Tutorial: Generative Adversarial Networks, arXiv: 1701.00160.
- [34] M.A. Nielsen and I.L. Chuang, *Quantum Computation and Quantum Information*, Cambridge University Press (2000)
- [35] M. Schuld, A. Bocharov, K. Svore, and N. Wiebe, Circuit-centric quantum classifiers, arXiv: 1804.00633.
- [36] W. Huggins, P. Patel, K.B. Whaley, and E.M. Stoudenmire, Towards quantum machine learning with tensor networks, arXiv: 1803.11537.
- [37] <https://pytorch.org/>
- [38] D.P. Kingma and J. Ba, Adam: A method for stochastic optimization, arXiv: 1412.6980.
- [39] J.F. Zeng, Y.F. Wu, J.G. Liu, L. Wang, and J.P. Hu, Learning and inference on generative adversarial quantum circuits, arXiv: 1808.03425.